Geolocation using TDOA and FDOA Measurements

Darko Mušicki

Independent Consultant

Entropy Data Pty Ltd

Email: Darko.Musicki@gmail.com

Wolfgang Koch

FGAN-FKIE

Wachtberg, Germany

Email: W.Koch@fgan.de

Abstract—Passive geolocaton of communication emitters provides great benefits to military and civilian surveillance and security operations. Time Difference of Arrival (TDOA) and Frequency Difference of Arrival (FDOA) measurement combination for stationary emitters may be obtained by sensors mounted on mobile platforms, for example on a pair of UAVs. Complex Ambiguity Function (CAF) of received complex signals can be efficiently calculated to provide required TDOA / FDOA measurement combination. TDOA and FDOA measurements are nonlinear in the sense that the emitter uncertainty given measurements in the Cartesian domain is non-Gaussian. Multiple non-linear measurements of emitter location need to be fused to provide the geolocation estimates. Gaussian Mixture Measurement (GMM) filter fuses nonlinear measurements as long as the uncertainty of each measurement in the surveillance (Cartesian) space is modeled by a Gaussian Mixture. Simulation results confirm this approach and compare it with geolocation using Bearings Only (BO) measurements.

Keywords: Tracking, data association, geolocation, nonlinear estimation, sensor fusion, TDOA, FDOA, GMM.

I. INTRODUCTION

Emitter location, in particular location of the emitters on the surface of the earth (geolocation), enables important applications, both military (surveillance) and civilian (localization, law enforcement, search and rescue, ...). For deep visibility of emitters, it is often advantageous to mount sensors on Unmanned Aerial Vehicles (UAVs). The limited size and weight of the hardware that can be carried by UAVs places an inherent limit on the types of the sensors that may be used, as well as their performance.

Emitter geolocation has two components. One is measurement, or choice of sensors, and the other is estimation/ information fusion, or processing of measurements provided by the sensors.

Passive geolocation has a long history, starting with the bearings only emitter localization. [1] is one of the first "modern" papers in this field.

For some time the passive geolocation using Time Difference of Arrival (TDOA) [2], [3] attracted the research attention. Using the TDOA measurements is especially suited to the geolocation of high-bandwidth emitters, e.g. radars. Knowing the time difference of arrival between the emitter and two sensors geolocalizes emitter to the points of a hyperbola. Introducing the third sensor (second TDOA measurement), one can geolocate the emitter at the intersection of two hyperbolae.

Another approach is to use two moving sensors, and non-linear estimation [4], [5] for geolocation using multiple TDOA measurements.

A combination of TDOA and Frequency Difference of Arrival (FDOA) is attractive for geolocation for several reasons. One is that only two sensors (two UAVs) need to be employed. The other is that TDOA and FDOA measurements are complementary in the sense that TDOA measurements are akin to the bearings measurements, and the FDOA measurements are akin to the range measurements. FDOA and TDOA measurements can be taken as the peak arguments of Complex Ambiguity Function (CAF) of the emitter signals received by the sensors. Efficient calculation of the CAF is presented in [6]. The Cramer Rao bound on the TDOA and FDOA measurement errors are frequently so small that equipment induced errors are predominant [7]. TDOA/FDOA observation criteria are discussed in [8].

TDOA/FDOA signals have been used for geolocation using satellites [7], [9]. These references concentrate on the errors obtained by a single measurement. This publication uses multiple TDOA/FDOA measurements for improved geolocation. Furthermore, it is assumed that the sensors are mounted on two UAVs. Geolocation results using Bearings Only (BO) measurements from the same UAVs are used for comparison.

Nonlinear estimation (information fusion) has been accomplished using the Gaussian Mixture presentation of Measurements (GMM) filter first published in [10]. Nonlinear measurements are preprocessed to Gaussian Mixture form in the observation space. Since both TDOA and FDOA (as well as the BO) measurements have the same form after the preprocessing, only one filter design is used to incorporate all three types of measurements, similar to the design in [4].

This paper is organized as follows. Problem statement is presented in Section II. TDOA and FDOA measurement acquisition using Complex Ambiguity Function is described in Section III. Section IV presents the GMM non-linear fusion algorithm as well as GMM presentation of TDOA and FDOA measurements in the observation space. The approach is validated using Simulations in Section V followed by the concluding remarks in Section VI.

II. PROBLEM STATEMENT

A stationary emitter on the surface of the earth needs to be geolocated. In this paper we assume a flat earth and furthermore assume that the sensors are located in the earth

---

plane. These assumptions considerably simplify the geometry, without influencing the conclusions. The earth curvature and geographical relief, and the height of the sensors can be accommodated in a straightforward manner.

Emitter state consists of position and speed, denoted here by e and v_e respectively

$$x = \begin{bmatrix} e & v_e \end{bmatrix}^T, \tag{1}$$

where $v_e = 0$ for the stationary emitter. Emitter trajectory at time k is modeled by

$$x_k = F_k x_{k-1} + \nu_k, \tag{2}$$

where the plant noise sequence ν_k is assumed to be a zero mean and white Gaussian sequence with covariance matrix Q_k, which is not correlated with any measurement noise sequence. For stationary emitters $F_k = I$ (identity matrix), and Q_k is a zero matrix. For filter stability reasons it is advisable to keep matrix Q determinant slightly above zero, though.

Two moving sensors are considered here. Their trajectories are assumed known, and are denoted here by:

$$x_i = \begin{bmatrix} s_i & v_i \end{bmatrix}^T, \ i = 1, 2 \tag{3}$$

where s_i and v_i denote known position and speed of sensor i respectively. Subscript k denoting time is implied and is omitted here for reasons of clarity. The radius vector between emitter and sensor i is given by:

$$r_i = e - s_i, \ i = 1, 2 \tag{4}$$

with the unit vector i_i equal to

$$i_i = \frac{r_i}{\|r_i\|} = \begin{bmatrix} \cos(\alpha_i) \\ \sin(\alpha_i) \end{bmatrix}, \ i = 1, 2 \tag{5}$$

A. Time Difference Of Arrival (TDOA)

Time Difference of Arrival measures the difference in arrival time $\Delta \tau_{1,2}$ from the emitter to the sensors. A typical situation is presented in Figure 1. True time difference of arrival is directly proportional to the difference in distance between the emitter and the sensors:

$$\Delta \tau_{1,2} = \Delta r_{1,2}/c = (\|r_1\| - \|r_2\|)/c, \tag{6}$$

where c denotes the speed of light. The function emitter position to time difference of arrival is of the many-to-one type. All points on the red dashed line in Figure 1 have the same distance difference to the two sensors, and therefore the same true time difference of arrival. This "constant TDOA" curve may be constructed by expressing equation (6) as a function of x and y emitter coordinates, and solving it. This is rather cumbersome, and in this paper we use the parametric constant TDOA curve construction. Consider the situation depicted on Figure 2. Assuming known angle α (the parameter), the following

$$\begin{aligned} \|r_1\| - \|r_2\| &= \Delta r_{1,2} \\ \|r_2\| \sin(\beta) &= \|r_1\| \sin(\alpha) \\ \|r_2\| \cos(\beta) - \|r_1\| \cos(\alpha) &= B \end{aligned} \tag{7}$$
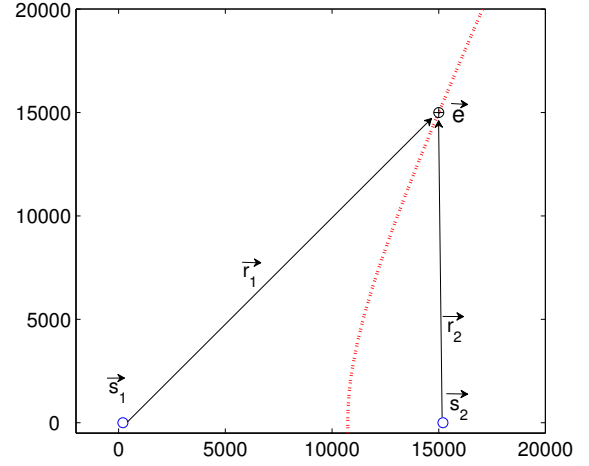

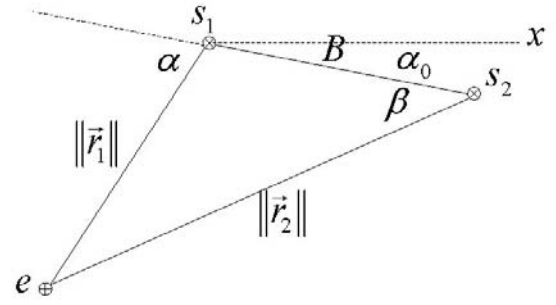Figure 1. TDOA scenario and constant TDOA emitter location curve

Figure 2. TDOA Geometry

holds and may be solved as

$$\|r_1(\alpha)\| = \frac{B^2 - (\Delta r_{1,2})^2}{2(-\Delta r_{1,2} - B \cos(\alpha))}, \tag{8}$$

where B denotes the baseline distance between the two sensors. Given parameter α, we can calculate $\|r_1\|$ and then the emitter location as

$$e(\alpha) = s_1 - \|r_1(\alpha)\| \begin{bmatrix} \cos(\alpha - \alpha_0) \\ \sin(\alpha - \alpha_0) \end{bmatrix}, \tag{9}$$

where α_0 denotes the slant angle of sensors baseline, as depicted on Figure 2. By letting α assume values from its range, the constant TDOA curve is constructed.

B. Frequency Difference of Arrival (FDOA)

Relative movement of sensor i to the emitter shifts the signal received by the sensor in frequency domain (the Doppler shift). Assuming a stationary emitter, the relative radial velocity of

the emitter and the corresponding Doppler shift are given by

$$v_{r,i} = - i_i^T v_i, \qquad\qquad i = 1, 2$$
$$\Delta f_i = - v_{r,i} f_0/c = i_i^T v_i f_0/c, \quad i = 1, 2, \qquad (10)$$

where f_0 denotes the carrier frequency and ^{T} denotes the matrix transpose. Subtracting the Doppler frequency shifts from different sensors, the Frequency Difference of Arrival equals

$$\Delta f_{1,2} = \Delta f_1 - \Delta f_2 = \left(i_1^T v_1 - i_2^T v_2 \right) f_0/c \qquad (11)$$

which is directly proportional to the differences in radial velocity

$$\Delta v_{r,1,2} = \Delta f_{1,2} c/f_0 = i_1^T v_1 - i_2^T v_2. \qquad (12)$$

Assuming known angle α_2, equation (12) is easily solved to yield

$$i_1^T v_1 \triangleq \|v_1\| \cos\left(\alpha_1 - \alpha_{v_1} \right) = \Delta v_{r,1,2} + i_2^T v_2$$
$$\alpha_1(\alpha_2) = \alpha_{v_1} + \arccos \frac{\Delta v_{r,1,2} + i_2^T v_2}{\|v_1\|}, \qquad (13)$$

where α_{v_1} denotes the angle of sensor 1 velocity vector. As the sensors positions are known, and given angles α_1 and α_2, the emitter location is calculated by triangulation. In other words, letting the angle α_2 assume values from its domain, equation (13) yields the "constant FDOA" curve. One example of the constant FDOA curve is shown by the red dashed curve on Figure 3, where the arrows sourced at sensors show the velocity direction of the sensors. By comparing Figure 1 with Figure 3, in this scenario TDOA signal takes the (approximate) role of bearings data, and the FDOA signal takes the (approximate) role of distance measurement.
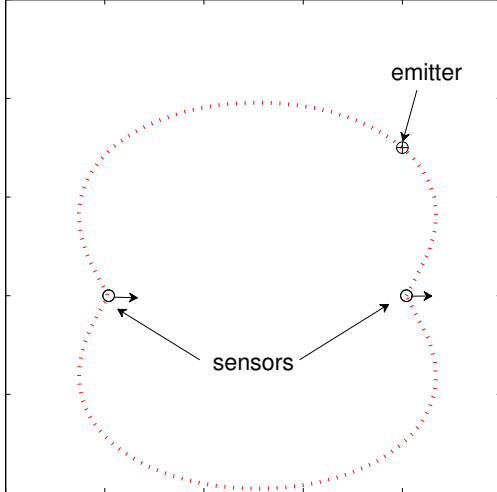

Figure 3. FDOA Scenario and constant FDOA emitter location curve

C. Deghosting

Figures 1 and 3 show that, for the sensor geometry depicted, both TDOA and FDOA uncertainty curves are symmetrical with respect to the sensor baseline. Therefore, a ghost target will be detected positioned symmetrical to the true target.

This ghost target may be removed by a number of means, including

- geometry. Often UAVs fly at the edge of the territory held by the antagonist, where the target positions are expected,
- additional bearings only sensor which only has to discriminate the ghost position,
- UAV maneuvers.

The choice of the deghosting method will, of course, depend on the logistics of the localization situation.

III. MEASUREMENTS

TDOA and FDOA measurements may be obtained by calculating the Complex Ambiguity Function (CAF). Complex Ambiguity Function cross correlates signals $s_1(t)$ and $s_2(t)$, received by sensors 1 and 2, parametrized by the lag τ, which is in fact the TDOA signal, and parametrized by the relative Doppler shift Δf, which is in fact the FDOA signal

$$A(\tau, \Delta f) = \int_0^T s_1(t) s_2^*(t + \tau) e^{2\pi j \Delta f t} \, dt, \qquad (14)$$

where $j = \sqrt{-1}$ denotes the imaginary unit. CAF is calculated for all applicable values of τ and Δf. TDOA and FDOA measurements are the arguments of the maximum complex envelope of the CAF:

$$\{\Delta \tau_m, \Delta f_m\} = \arg_{\tau, \Delta f} \max\left(A(\tau, \Delta f) \right). \qquad (15)$$

Equation (14) seems to have prohibitively high computational complexity, having to calculate integrals for all applicable values of two dimensional parameters. In fact, assuming a communication signal being emitted as described in Section V, [6] describes a computationally efficient procedure to calculate CAF, which is well within current state of the art. Complex signal samples need to be broadcast to the fusion center which calculates CAF, for majority of communication signals the required bandwidth is available now.

TDOA and FDOA measurements may be modeled as

$$\Delta \tau_m = \Delta \tau_{1,2} + \nu_{\Delta \tau}$$
$$\Delta f_m = \Delta f_{1,2} + \nu_{\Delta f} \qquad (16)$$

where measurement error processes $\nu_{\Delta \tau}$ and $\nu_{\Delta f}$ are assumed to be zero mean, white and mutually uncorrelated with rms values of $\sigma_{\Delta \tau_m}$ and $\sigma_{\Delta f_m}$ respectively. Multiplying the TDOA and FDOA measurement equations (16) by c and c/f_0 respectively

$$\Delta r_m = \Delta r_{1,2} + \nu_{\Delta r}$$
$$\Delta v_m = \Delta v_{r,1,2} + \nu_{\Delta v} \qquad (17)$$

with measurement error processes $\nu_{\Delta r}$ and $\nu_{\Delta v}$ assumed to be zero mean, white and mutually uncorrelated with rms values of $\sigma_{\Delta r} = c \cdot \sigma_{\Delta \tau_m}$ and $\sigma_{\Delta v} = c \cdot \sigma_{\Delta f_m}/f_0$ respectively.

Reference [6] shows that the TDOA and FDOA measurements obtained by equations (14) and (15) are efficient in the Cramer-Rao sense. Rms TDOA and FDOA measurement errors are given by

$$\begin{aligned} \sigma_{\Delta \tau_m}^{-1} &= \beta \sqrt{BTS_i} \\ \sigma_{\Delta f_m}^{-1} &= T_e \sqrt{BTS_i} \end{aligned} \qquad (18)$$

respectively, where B denotes the signal bandwidth, T denotes the integration period, and S_i denotes the input signal to noise ratio. Rms bandwidth and signal duration are denoted by β and T_e and are defined by

$$\begin{aligned} \beta &= 2\pi \sqrt{\frac{\int_{-\infty}^{\infty} f^2 W_s(f) df}{\int_{-\infty}^{\infty} W_s(f) df}} \\ T_e &= 2\pi \sqrt{\frac{\int_{-\infty}^{\infty} t^2 |u(t)|^2 dt}{\int_{-\infty}^{\infty} |u(t)|^2 dt}}, \end{aligned} \qquad (19)$$

where $W_s(f)$ denotes the signal power spectrum, and $|u(t)|$ denotes the signal envelope. As shown in [6] and in Section V, the TDOA and FDOA rms errors are very small, even in the case of modest input signal to noise ratio. Practically achievable measurement errors also depend on the stability of other components in the signal processing chain, which is beyond the scope of this paper. It should be mentioned that UAV ownship position and speed errors also increase the measurement errors in the obvious fashion, the full analysis of this effect is also outside the scope of this paper.

To accommodate for imperfect equipment, simulations carried out in Section V assume rms measurement errors significantly above the theoretical limits defined by equation (18).

IV. NONLINEAR MEASUREMENT FUSION

Passive measurements generally have non-Gaussian uncertainty in the observation space, i.e. they usually are non-linear. In the measurement space, TDOA and FDOA true value uncertainties, given the measurement, are Gaussian, as per equations (16) and (17). However, the transformation into the observation linear space, in this case the two-dimensional Cartesian plane, results in very non-Gaussian probability density functions (pdfs), as indicated by the uncertainty curves on Figures 1 and 3. Estimation using these measurements becomes non-linear information fusion, which in this work is performed using the Gaussian Measurement Mixture (GMM) algorithm, first published in [10].

GMM filter is based on the notion that any probability density function (pdf) may be modeled by a Gaussian mixture [11]. Estimated pdf based on non-linear (non-Gaussian) measurements is also non-Gaussian. Thus both state estimate and the observation space measurement pdfs need to be modeled by Gaussian mixtures. Each element of the Gaussian mixture is termed here a "component". State estimate here is termed a "track".

A. GMM filter

In this application both TDOA and FDOA measurements arrive simultaneously at time k, as per equation (15). One way to use both measurements is to introduce a "dummy" time $k+1$, with zero seconds of physical time between time k and $k+1$. First the GMM estimate based on the TDOA measurement is updated at time k, and then the GMM prediction is applied between time k and $k+1$, and finally the FDOA measurement is applied to update the GMM state estimate at time $k+1$. As the time interval between samples k and $k+1$ is zero, GMM prediction at time $k+1$ is identical to GMM estimate at time k.

Denote by z_k the measurement received at time k (either TDOA or FDOA in this case), and by Z^k the set of all measurements received up to and including the measurement received at time k.

A posteriori track pdf at time $k-1$ (after processing the measurement z_{k-1}) is a Gaussian mixture, given by

$$\begin{aligned} p\left(x_{k-1}|Z^{k-1}\right) &= \\ &= \sum_{c=1}^{C_k} \xi(c) \mathcal{N}\left(x_{k-1}; \hat{x}_{k-1|k-1}(c), P_{k-1|k-1}(c)\right) \end{aligned} \qquad (20)$$

where c is the index into track components, C_k denotes the number of track components, $\mathcal{N}(x; m, P)$ denotes the Gaussian pdf of variable x with mean value m and covariance matrix P, and $\hat{x}_{k-1|k-1}(c)$ and $P_{k-1|k-1}(c)$ are the mean and covariance of track component c, with the constraint of

$$\sum_{c=1}^{C_k} \xi(c) = 1; \ \xi(c) \geq 0. \qquad (21)$$

Chapman-Kolmogoroff equation is linear, thus the track state prediction at time k is

$$p\left(x_k|Z^{k-1}\right) = \sum_{c=1}^{C_k} \xi(c) \mathcal{N}\left(x_k; \hat{x}_{k|k-1}(c), P_{k|k-1}(c)\right) \qquad (22)$$

where each component c is propagated in a linear manner

$$\begin{aligned} \left[\hat{x}_{k|k-1}(c), P_{k|k-1}(c)\right] &= \\ KF_P\left(\hat{x}_{k-1|k-1}(c), P_{k-1|k-1}(c), F, Q\right), \end{aligned} \qquad (23)$$

where KF_P denotes the linear Kalman filter propagation. If the time interval between $k-1$ and k is zero, KF_P becomes the identity operation.

Measurement uncertainty in the observation space is also represented as a Gaussian Mixture

$$p\left(y_k\right) = \sum_{g=1}^{G_k} \gamma(g) \mathcal{N}\left(yk; \hat{y}_k(g), R_k(g)\right) \qquad (24)$$

where g is the index into measurement components, G_k denotes the number of measurement components, and $\hat{y}_k(g)$ and $R_k(g)$ are the mean and covariance of measurement component g, with the constraint of

$$\sum_{g=1}^{G_k} \gamma(g) = 1; \ \gamma(g) \geq 0 \qquad (25)$$

Each measurement component g uses Kalman Filter update of each track component c to create one component of the *a posteriori* track pdf. Thus the number of components in the *a posteriori* track pdf at time k is $C_k \cdot G_k$ and the *a posteriori* track state pdf is given by

$$p\left(x_k | Z^k\right) = \sum_{c^+=1}^{C_k G_k} \xi(c^+) \mathcal{N}\left(x_k; \hat{x}_{k|k}(c^+), P_{k|k}(c^+)\right) \quad (26)$$

where $c^+ \equiv \{g, c\}$ is the index into *a posteriori* track components, and $\hat{x}_{k|k}(c^+)$ and $P_{k|k}(c^+)$ are the mean value and covariance matrix of component c^+ respectively, calculated as

$$\begin{aligned}
\left[\hat{x}_{k|k}(c^+), P_{k|k}(c^+)\right] = \\
KF_E\left(\hat{x}_{k|k-1}(c), P_{k|k-1}(c), \hat{y}_k(g), R_k(g), H\right),
\end{aligned} \quad (27)$$

where KF_E denotes the standard linear Kalman filter estimation operation. Relative probabilities $\xi(c^+) \equiv \xi(\{g, c\})$ satisfy

$$\begin{aligned}
\xi(c^+) &\propto \xi(c)\gamma(g)\, \mathcal{N}(\hat{y}_k(g); H\hat{x}_{k|k-1}(c), S_k(c^+)) \\
&\sum_{c=1}^{C_k} \sum_{g=1}^{G_k} \xi(c^+) = 1,
\end{aligned} \quad (28)$$

where

$$S_k(c^+) = HP_{k|k-1}(c)H^T + R_k(g) \quad (29)$$

Output state estimate mean and covariance is the mean and covariance of Gaussian mixture

$$\begin{aligned}
\left[\hat{x}_{k|k}, P_{k|k}\right] = \\
GM\left(\left[\hat{x}_{k|k}(c^+), P_{k|k}(c^+), \xi(c^+)\right]_{c^+=1}^{C_k G_k}\right).
\end{aligned} \quad (30)$$

Left unchecked the number of track components increases exponentially which quickly exhausts available computational resources. Thus track component management [12], [13] in the form of pruning and/or merging is a prerequisite for any GMM practical implementation.

B. TDOA/FDOA measurement GMM presentation

The same procedure is used for GMM presentation of both TDOA and FDOA measurements. In this section TDOA measurement symbols only are used.

The first step involves mapping the measurements into $\pm\sigma$ regions in the surveillance domain. It involves drawing two parametric uncertainty curves. The values of $\Delta\tau_m \pm \sigma_{\Delta\tau_m}$ are used. The result is shown in Figure 4. TDOA $\pm\sigma$ region is delimited by the blue lines, and needs to be represented by a set of non-overlapping ellipsoids representing the 1σ footprints of TDOA measurement components.

This procedure starts by dividing each uncertainty curve by a set of points, where both sets have the same cardinality. Then an ellipsis is inscribed within each quadrangle formed by one pair of points on each uncertainty curve on Figure 4. Assume that points x_1 and x_2 are on one curve, and points x_3 and x_4 are on the other curve, and we want to define the measurement component g whose footprint is the inscribed ellipsis. The measurement component is defined by its mean $\hat{y}_k(g)$ and covariance $R_k(g)$.
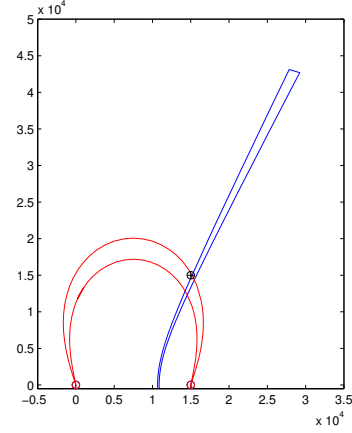

Figure 4. TDOA (blue) and FDOA (red) $\pm\sigma$ emitter location uncertainty

The end points of one semi axis of the inscribed ellipsis are defined by

$$\begin{aligned}
x_{c1} &= (x_1 + x_3)/2 \\
x_{c2} &= (x_2 + x_4)/2.
\end{aligned} \quad (31)$$

The length and the angle of one semi-axis of the ellipsis are given by

$$\begin{aligned}
\Delta x_c &= x_{c1} - x_{c2} \\
D_c &= \|\Delta x_c\|/2 \\
i(\alpha_c) &\triangleq \begin{bmatrix} \cos(\alpha_c) & \sin(\alpha_c) \end{bmatrix} = \Delta x_c/\|\Delta x_c\|.
\end{aligned} \quad (32)$$

The length of the other semi axis is given by

$$\begin{aligned}
D_s &= \begin{bmatrix} -\sin(\alpha_c) & \cos(\alpha_c) \end{bmatrix} \\
&\quad ((x_1 - x_3)/2 + (x_2 - x_4)/2)/2 \\
&= i(\alpha_c + \pi/2)^T (x_1 + x_2 - x_3 - x_4)/4.
\end{aligned} \quad (33)$$

Denote by $T(\alpha) = \begin{bmatrix} i(\alpha) & i(\alpha + \pi/2) \end{bmatrix}$ the α rotation matrix. Then the center of the inscribed ellipsis is given by

$$\hat{y}_k(g) = 0.5(x_{c1} + x_{c2}), \quad (34)$$

which is also the mean of the measurement component corresponding to the ellipsis. The covariance matrix of the measurement component is given by.

$$R_k(g) = T(\alpha_c) \begin{bmatrix} D_c^2 & 0 \\ 0 & D_s^2 \end{bmatrix} T(\alpha_c)^T. \quad (35)$$

The end result of following this procedure to transform the TDOA and FDOA measurement uncertainties from Figure 4 is shown on Figure 5, where each measurement component is represented by its ellipsis footprint.

Without any prior information, the emitter position is equally probable at any point of the observation space. Therefore, the probability that the emitter is within the footprint of a measurement component is proportional to the area of the footprint:

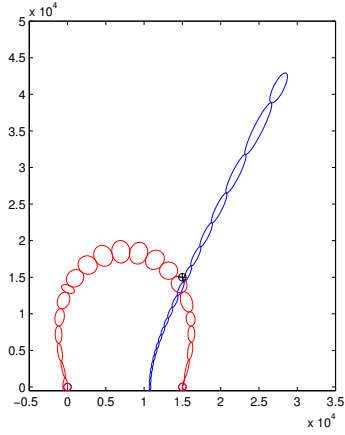$$\gamma(g) \propto \sqrt{|R_k(g)|}. \quad (36)$$

Figure 5. TDOA (blue) and FDOA (red) emitter location uncertainty GMM presentation

V. Simulations

An emitter geolocation scenario using sensors mounted on two UAVs is simulated. Figure 6 shows the position of the sensors and the emitter as the first measurement is taken. The stationary emitter is assumed to be on the surface of the (flat) earth, and the UAVs are flying due east (positive x axis direction) with the uniform speed of $100m/s$, and the initial positions of $\begin{bmatrix} 0 & 0 \end{bmatrix} km$ and $\begin{bmatrix} 15 & 0 \end{bmatrix} km$. The two UAVs
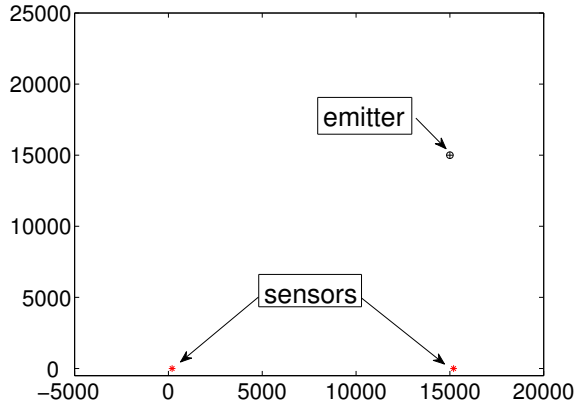

Figure 6. Geolocation scenario

measure both the bearings of the input signal and the complex signal. The CAF of the signals collected by the two UAVs is calculated, and the arguments of the peak of CAF are the TDOA and FDOA measurements. The CAF integration time of 2 seconds equals the measurement sampling time.

Input signal to noise ratio is assumed to be $\gamma_i = 0dB$, its bandwidth is $B = 25kHz$, and effective time integration is $T = 2s$ per CAF measurement sample. According to equations (18)-(19) the minimum measurement rms errors for TDOA and FDOA are $\sigma_\tau = 98ns$ and $\sigma_{\Delta f} = 1.2mHz$ respectively. Assuming the carrier frequency of $f_0 = 100MHz$, this

translates into the differential position and speed rms errors of $\sigma_{\Delta r} = 30m$ and $\sigma_{\Delta v} = 3.7mm/s$ respectively. To account for various equipment imperfections and sensor position uncertainties, in the simulations we anticipate measurement rms errors much higher than the theoretical limits. One set of measurements is generated assuming rms measurement errors of $\sigma_{\Delta r} = 100m$ and $\sigma_{\Delta v} = 1m/s$, and is labeled here "fine". The other set of measurements assumes rms measurement errors of $\sigma_{\Delta r} = 200m$ and $\sigma_{\Delta v} = 4m/s$, and is labeled here "coarse".

The accuracy of the bearings measurements depend on the size of the antennas. Due to the small size of antennas which may be fitted on the UAVs, the bearings rms measurement errors are assumed to be $\sigma_\theta = 5°$. Significant elevation dependent bias is also present in the BO measurements due to the inevitable presence of UAV metal parts near the antennas, however this issue is ignored here and the bias is assumed to be zero. BO measurements are also processed using a GMM filter, as described in [14].

GMM filter used both merging and pruning to control the number of track components, which converged toward a total of 20 track components in the case TDOA/FDOA measurements, and toward a total of 8 track components in the case of BO measurements.

Measurement uncertainties are modeled as Gaussian Mixtures. Bearings only measurements have 5 Gaussian components each, as presented in [15]. TDOA and FDOA measurements Gaussian Mixture have 20 components each. Fine and coarse TDOA and FDOA measurement uncertainties are depicted on Figure 7, where each Gaussian pdf component of the mixture is represented by its footprint ellipse.

Geolocation results are presented in Figure 8 which presents root mean square errors based on 1000 simulation runs. Figure 8(a) shows the full scale errors, whereas Figure 8(b) zooms in to show final details of TDOA/FDOA combination geolocation errors. Geolocation errors based on BO measurements remain too high (more than $700m$) to be of practical use. TDOA/FDOA fine and coarse measurement combinations result in geolocation errors which are less than $50m$ and $200m$ respectively. Furthermore, when using the fine TDOA/FDOA measurement errors, the geolocation errors drop to less than $100m$ in less than 10 measurement samples, or in less than $20s$.

VI. Conclusions

In this paper the GMM filter has been used as a non-linear fusion estimator. It incorporates nonlinear measurements from various sensor types, as long as they are represented as the Gaussian Mixture. Of course, the observability criteria for measurements have to be observed.

GMM has been applied to the problem of geolocation of stationary emitter of communication signals. TDOA and FDOA measurements are assumed to be obtained using the Complex Ambiguity Function [6] processing, and BO measurements are assumed to measured directly.
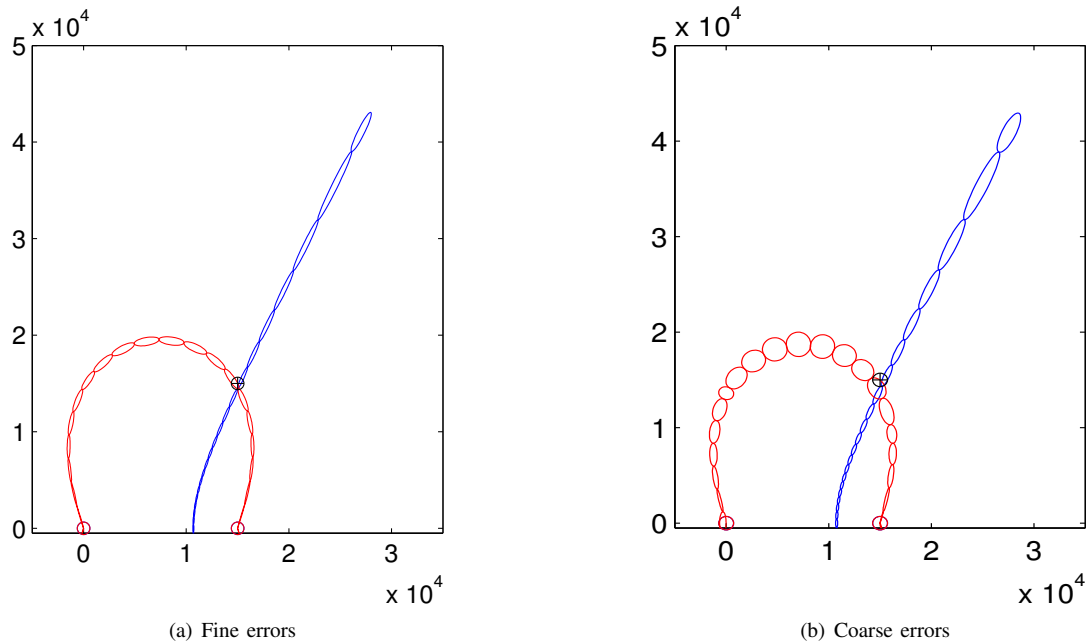
(a) Fine errors

(b) Coarse errors

Figure 7.   GMM conversion of the emitter location uncertainty. Blue: TDOA. Red: FDOA.

(a) RMS errors
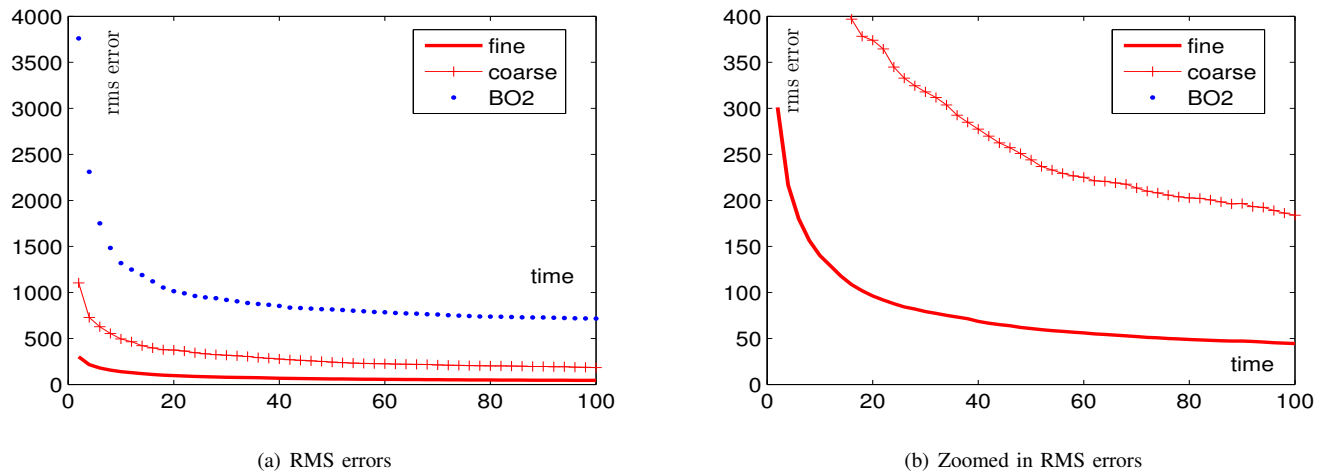

(b) Zoomed in RMS errors

Figure 8.   RMS estimation errors.

Simulation results show the validity of this approach. Although the rms measurement errors were significantly larger than the theoretical minimum, final geolocation estimates are reduced by an order of magnitude compared to the BO measurements.

REFERENCES

[1] R. Stansfield, "Statistical theory of DF fixing," *Journal of IEE*, vol. 94, no. 15, pp. 762–770, 1947.

[2] M. Schmidt, "A new approach to geometry of range difference location," *IEEE Trans. Aerospace and Electronic Systems*, vol. 8, no. 6, pp. 821–835, November 1972.

[3] K. Ho and Y. Chan, "Solution and performance analysis of geolocation by tdoa," *IEEE Trans. Aerospace and Electronic Systems*, vol. 29, no. 4, pp. 1311–1322, October 1993.

[4] N. Okello and D. Mušicki, "Measurement association and tracking for emitter localisation using paired UAVs," *Journal of Advances in Information Fusion (submitted)*.

[5] F. Fletcher, B. Ristic, and D. Mušicki, "TDOA measurements from two UAVs," in *10th International Conference on Information Fusion, Fusion 2007*, Quebec, Canada, July 2007.

[6] S. Stein, "Algorithms for ambiguity function processing," *IEEE Trans. Acoustic, Speech and Signal Processing*, vol. 29, no. 3, pp. 588–599, June 1981.

[7] R. Bardelli, D. Haworth, and N. Smith, "Interference localisation for the Eutelsat satellite system," in *Global Telecommunications Conference, GLOBECOM '95*, vol. 3, Singapore, November 1995, pp. 1641–1651.

[8] P. Chestnut, "Emitter location accuracy using tdoa and differential doppler," *IEEE Trans. Aerospace and Electronic Systems*, vol. 18, no. 2, pp. 214–218, March 1982.

[9] J. Kaufmann and W. Hutchinson, *Emitter Location with LES-9/9 Using Differential Time of Arrival and Differential Doppler Shift*.   Report 698 (Rev. 1), Lincoln Laboratory, MIT, Lexington, Massachusetts, 2000.

[10] D. Mušicki and R. Evans, "Measurement Gaussian sum mixture target tracking," in *9th International Conference on Information Fusion, Fusion 2006*, Florence, Italy, July 2006.

[11] D. L. Alspach and H. W. Sorenson, "Nonlinear bayesian estimation using gaussian sum approximation," *IEEE Trans. Automatic Control*, vol. 17, no. 4, pp. 439–448, Apr 1972.

[12] S. Blackman and R. Popoli, *Design and Analysis of Modern Tracking Systems*. Artech House, 1999.

[13] D. J. Salmond, "Mixture reduction algorithms for target tracking in clutter," in *SPIE: Signal and Data Processing of Small Targets*, vol. 1305, Orlando, Florida, April 1990, pp. 434–445.

[14] D. Mušicki, "Multi-target tracking using multiple passive bearings-only asynchronous sensors," *IEEE Trans. Aerospace and Electronic Systems (accepted for publishing)*.

[15] ——, "Bearings only multi-sensor maneuvering target tracking," *Systems Control Letters*, vol. 57, no. 3, pp. 216–221, March 2008.